Advances in Aerodynamics

RESEARCH Open Access

Study on atomization characteristics of a kerosene jet in a supersonic crossflow

Yi Zhang[1], Jialing Le[1] and Ye Tian[1*]

*Correspondence:
tianye@cardc.cn

[1] China Aerodynamics Research and Development Center, Mianyang 621000, China

Abstract

The combustion performance of a scramjet engine is based on a two-phase mixing process of its fuel. To elucidate the mechanism of jet atomization in supersonic airflows, a numerical simulation of liquid jet atomization in a supersonic crossflow is carried out. The Euler method is used to calculate the gas phase, while the Lagrangian particle tracking method is used to calculate the liquid phase. The Reitz wave model is used to simulate the first breakup of the liquid jet, and the Kelvin-Helmholtz/Rayleigh-Taylor hybrid breakup model is used to simulate the second breakup of the droplets. The influence of the liquid/gas momentum flux ratio and the diameter of the jet on the atomization characteristics is discussed. The results show that the penetration depth increases with increasing nozzle diameter and liquid/gas momentum flux ratio. A jet with a larger liquid/gas momentum flux ratio breaks faster, and its Sauter mean diameter is smaller. The Sauter mean diameter of a droplet decreases with decreasing nozzle diameter. At 30 mm downstream of the nozzle, all jets are basically atomized, and the SMD of the jet is around 10 μm. The nozzle diameter has a greater influence on the jet penetration depth than does the liquid/gas momentum flux ratio.

Keywords: Supersonic flow, Numerical simulation, Atomization, Penetration depth, Liquid jet

1 Introduction

The scramjet is set to be a very important aspirated propulsion system in future aspirated supersonic aircraft [1, 2]. Scramjet design depends on the combustion flow mechanism. The combustor is the most complex and important part in the scramjet engine. Different from using gaseous fuel, the scramjet engine uses liquid hydrocarbon fuel, which has to undergo atomization, breakup, mixing, and other processes. This constitutes an overall complex process involving multi-scale, multi-phase, and multi-physical field coupling [3, 4]. Combustion in a scramjet combustor is carried out in a supersonic crossflow, and the time taken for the airflow to pass through the combustor is usually only a few milliseconds. However, during the fuel injection process, the atomization of liquid fuel, as well as the collision of droplets after atomization, evaporation, and mixing with the supersonic airflow, takes longer. This means that the fuel and air mix together with difficulty. It is difficult to ignite and stabilize the combustion of two-phase mixtures in supersonic flows. For an engine that uses liquid fuel, atomization is the first step in

achieving the mixing of fuel and air and forms the basis of combustion. The quality of atomization is related to the combustion performance of the engine. If the atomization is good, the diameter of the atomized fuel is small and uniform, which is conducive to the mixing of fuel and air, which is then, in turn, conducive to combustion. Therefore, it is of great significance to study the atomization and mixing characteristics of the fuel jet in a scramjet combustor.

Liquid breaking in a supersonic crossflow can be divided into three main parts: the liquid column, the liquid ligament, and the liquid drop [5]. When liquid is injected into an airflow, a KH instability occurs at the gas-liquid interface, causing RT instability. This eventually leads to the formation of large droplets and liquid filaments, constituting the primary breakup of the liquid jet. The aerodynamic instability caused by the relative velocity between phases further breaks droplets and ligaments into smaller droplets. This process is a secondary breakup process. The small droplets formed are the basis for the successful completion of combustion in supersonic crossflows [6]. Wu et al. [7] used the PDPA method to study the atomization of water jets in a subsonic crossflow. When the liquid-gas momentum flux ratio was small, large droplets were concentrated in the central part, and when it was large, they were concentrated at the top. The cross-section increases with increasing jet velocity and nozzle diameter and decreasing incoming flow velocity. Kush and Schetz [8] studied transverse injections of water, carbon disulfide, 30% glycerol solution, and Freon in Mach 2.4 and 4.0 airflows using high-speed photography and spark shadowing. The jet broke quickly in the near field and broke into small droplets in the far field. The breakup position is usually located at the sound velocity point of the bow shock wave. Mach number, liquid viscosity, surface tension, and liquid vapor pressure have little effect on the primary breakup. The rectangular orifice breaks faster than the circular orifice. Wei et al. [9] used different optical measurement methods to analyze the influence of nozzle diameter, quantity and distribution, fuel injection pressure, nozzle diameter, and crossflow Mach number on the penetration depth of kerosene and on the droplet size in a subsonic airflow. The fuel injection pressure drop and crossflow Mach number were positively correlated with the atomization performance, while the nozzle diameter was negatively correlated with it. Wu et al. [10] used a phase Doppler particle analyzer to conduct an experimental study on transverse water jets in supersonic airflows. The SMD (Sauter Mean Diameter) distribution of droplets on the cross-section changed from type C to type I along the flow direction; that is, the droplet distribution gradually became uniform due to the fragmentation of large droplets and the polymerization of small droplets throughout the entire atomization process. Kolpin et al. [11] used a schlieren method to study the penetration depth and spanwise distribution of jets in a supersonic crossflow with an injection angle. Their analytical models that described the penetration depth and spanwise distribution exhibited differences compared with their own experimental results. This meant that the penetration depth and spanwise distribution of the jets were greatly affected by experimental conditions.

Reitz and Diwakar [12] assumed that atomization and droplet breaking were inseparable processes in the dense spray near a nozzle. Atomization was achieved by injecting blobs equal to the diameter of the nozzle and spraying droplets with similar physical properties using a random injection method. Considering droplet

fragmentation, collision, polymerization, and its influence on airflow turbulence, the calculated spray core length was in good agreement with the measured results. Secondary droplet atomization models include the TAB model [13], the Reitz wave model [14], the KH-RT hybrid model [15], and the improved model based on the above models [16–20]. Fan et al. [21] examined three classical breakup models under a supersonic airflow, namely the TAB model, the Reitz wave model, and the KH-RT hybrid model. The KH-RT (hybrid) model had the highest accuracy in predicting penetration depth and drop diameter distribution. Reitz and Diwakar [22] adopted a mixed model comprising RT and KH to simulate the jet breakup process, improving the accuracy of spray simulation. Lin et al. [23, 24] conducted systematic experimental research on jet atomization in supersonic airflows. The study covered the influence of liquid physical properties, nozzle diameter, injection angle, gas-liquid mass flow ratio, gas-liquid momentum flux ratio, and other factors on atomization. Im et al. [25] adopted the improved KH-RT hybrid model, in which the KH breakup length was corrected by the breakup time and mass equation. The calculated results were compared with those of the TAB model. The TAB model was shown to be unsuitable for high-speed jets, and the model adopted in this paper is more accurate. Shock waves have been found to influence atomization. Beale and Reitz [26] modified the KH-RT hybrid model so that the RT instability affected all droplets in the periphery of the jet core. They adopted the KH model to predict the primary breakup process of a diesel jet, the TAB model to simulate the droplet deformation, and the KH-RT hybrid model to simulate the secondary breakup process. Only droplets outside the breakup length were affected by the RT instability. A Rosin-Rammler (R-R) distribution was used to specify the size of a child droplet after the parent droplet broke. The additional RT instability significantly improved the temperature dependence of the liquid penetration depth. Wang et al. [27] improved the KH-RT hybrid model and optimized the empirical parameters added to the model. The KH breakup model had more control over the entire liquid jet breakup process than the RT breakup model. Moreover, the B_0 parameter of the KH model had a significant impact on the downstream SMD distribution. Li et al. [28–30] modified the drag coefficient and spray breakup model by using the Euler-Lagrange method and taking into account the compressibility effect and deformation of droplets. Droplet stripping from a liquid column was calculated using the KH breakup model, and a numerical simulation of a liquid jet in a gas crossflow with a Mach number of 1.94 was carried out using the RT and TAB models competitively during the secondary breakup process. The numerical simulation results were in good agreement with the experimental results, and a jet spray trailing phenomenon was successfully revealed experimentally. Huang et al. reviewed the effects of nozzle parameters [31], injection schemes [32–34], and engine geometric parameters [35] on enhancing fuel mixing and combustion stability, providing ideas for the design of scramjet combustion chambers. Much work has been conducted on factors affecting atomization characteristics, such as the jet penetration depth [10], droplet velocity distribution [36], and particle size distribution [37, 38]. It includes the gas-liquid momentum ratio [39–41], injection pressure [9], nozzle shape [42], jet quantity and position [43], jet physical property parameters [44], and jet angle [45, 46]. Overall, the purpose of the research is to identify parameter combinations that can improve the mixing and

combustion performance of fuel and incoming flow in scramjet engines, providing ideas for the design of scramjet engines with high flight Mach numbers.

After entering the supersonic transverse airflow, the liquid undergoes deformation and then undergoes surface fragmentation, with small droplets peeling off from the surface of the liquid column. Most numerical simulations do not simulate this process. In this article, we use the Reitz wave growth model to simulate surface fragmentation, while improving the mixed breakup model proposed by Patterson and Reitz. The start of secondary breakup is controlled by the breakup length, and surface breakup occurs within the breakup length. The length of breakup is derived from experiments.

The liquid/gas momentum flux ratio has an important impact on the flow filed structure, shock wave intensity, and jet penetration trajectory in the jet region. Penetration depth is an important indicator of fuel atomization mixing. And the diameter of the nozzle is an important influencing factor for changing the fuel mass flow rate. Therefore, this article investigates the effects of liquid/gas momentum flux ratio and nozzle diameter on the atomization characteristics of liquid fuel. In this paper, an atomization model is first introduced. Then, jet atomization is numerically simulated to study the atomization characteristics of the vertical injection of a kerosene jet into a supersonic crossflow.

2 Calculation method

The calculation in this paper is based on the self-developed AHL3D computing platform, and its accuracy has been verified elsewhere [47, 48]. The Euler-Lagrange method was used for calculation. The governing equation of the gas phase was a three-dimensional Reynolds-averaged Navier-Stokes (RANS) equation in an Eulerian coordinate system, and the Lagrange method was used for the liquid phase. The exchange of mass, momentum, and energy between gas and liquid phases was added to the equation through the source term. In the Lagrange method, a droplet was treated as a point particle with mass and momentum but no volume.

The gas phase governing equation in Cartesian coordinates, with conservation of mass, momentum, and energy, is:

$$\frac{\partial Q}{\partial t}+\frac{\partial F}{\partial x}+\frac{\partial G}{\partial y}+\frac{\partial E}{\partial z}=\frac{\partial F_v}{\partial x}+\frac{\partial G_v}{\partial y}+\frac{\partial E_v}{\partial z}+S_g+S_l. \tag{1}$$

Where $Q=(\rho,\rho u,\rho v,\rho w,\rho E,\rho c_i)^T$, E, F, and G are the inviscid flux; F_v, G_v, and E_v are the viscous flux; and S_g is the gas phase chemical reaction source term. The total internal energy of a gas $E_t=e+\frac{1}{2}(u^2+v^2+w^2)$; e is the internal thermodynamic energy of the gas, and S_l is the gas-liquid coupling source term. u, v, and w are the velocity components of the gas in the x-, y-, and z-directions, respectively. ρ is the density of the gas.

The flow field in a scramjet engine is a high Reynolds number turbulent flow field, and fuel mixing and combustion are complex turbulent processes. Therefore, turbulence models applied to flow field calculations must be able to simulate the effects of anisotropic turbulent shear forces, turbulence separation and compressibility on the turbulent flow, as well as the interaction between chemical reactions and turbulence. When particles are in a turbulent flow field, they are affected by the diffusion of turbulence. Turbulence model [49] and turbulent dispersion have an impact on the trajectory of the jet. Kumaran and Badu [50] studied the effect of turbulent dispersion on mixing and

found that droplet dispersion caused by turbulent flow can enhance mixing. The turbulence model used in this article is a TNT $k-\omega$ dual equation turbulence model, whose control equation is

$$\begin{gathered}\frac{\partial}{\partial t}\begin{pmatrix}\rho k\\ \rho w\end{pmatrix}+\frac{\partial}{\partial x_i}\begin{pmatrix}\rho k u_i\\ \rho w u_i\end{pmatrix}=\frac{\partial}{\partial x_i}\begin{pmatrix}\mu_k\frac{\partial k}{\partial x_i}\\ \mu_w\frac{\partial w}{\partial x_i}\end{pmatrix}+\begin{bmatrix}P_k-D_k\\ P_\omega-D_\omega+D_c\end{bmatrix},\\ \mu_t=\rho k/\omega.\end{gathered} \tag{2}$$

P_k and $P_\omega=\alpha_\omega\left(\frac{\omega}{\kappa}\right)P_k$ are the turbulence generation terms. $D_k=\beta_k\rho\omega k$ and $D_\omega=\beta_w\rho\omega^2$ are the damage terms. $D_c=\sigma_d\frac{\rho}{\omega}\max(\nabla k\cdot\nabla\omega,0)$ is the cross dissipation term. $\mu_k=(\mu+\sigma_k\mu_t)$, and $\mu_\omega=(\mu+\sigma_\omega\mu_t)$.

The liquid phase traces the position of a droplet by solving the particle motion equation in a Lagrangian coordinate system. It can be expressed using the Basset-Boussinesq-Oseen equation. In a supersonic two-phase flow, gravity, volume force, pressure, Basset force, etc. are all relatively small compared to resistance and can be ignored. Under these assumptions, the position and velocity equations of particles are:

$$\frac{d\vec{X}}{dt}=\vec{V}_d, \tag{3}$$

$$m_d\frac{dV_d}{dt}=\vec{F}_{dr}, \tag{4}$$

$$\vec{F}_{dr}=\frac{1}{2}C_d\rho A_d\left|\vec{V}-\vec{V}_d\right|(\vec{V}-\vec{V}_d), \tag{5}$$

where $\vec{V}_d$ is the droplet velocity, denoted as $\vec{V}_d=(u_d,v_{d,}w_d)$, $\vec{F}_{dr}$ is the droplet drag force, and $\vec{V}$ is the gas phase velocity, denoted as $\vec{V}=(u,v,w)$. A_d is the droplet cross-sectional area, and C_d is the drag coefficient. The formula is:

$$C_d=\begin{cases}\frac{24}{Re_r}(1+\frac{Re_r^{2/3}}{6}), & Re_r<1000,\\ 0.44, & 1000<Re_r<3\times10^5,\end{cases} \tag{6}$$

where Re_r is the relative Reynolds number, expressed as $Re_r=\rho d_d\left|\vec{V}-\vec{V}_d\right|/\mu$.

The control equations were discretized using the finite volume method, the inviscid flux is in the Steger Warming format, the time advance was obtained using the implicit Lower-Upper Symmetric Gauss Seidel (LU-SGS) method, and the unsteady calculation was performed using the double time step method. For the spray calculation, the discrete droplet model was used. A large amount of computation would have been required to track each individual droplet. Therefore, to save on computational resources and for computational feasibility, a Monte-Carlo method was used. This permitted the simulation of a large number of droplets with a relatively low computational cost. Each calculated droplet represented a large number of droplets with the same properties. The governing equation of the droplet phase was solved using Runge-Kutta methods.

Our atomization model adopted the hybrid breakup model of Patterson and Reitz. In the dense spray area near the nozzle, the "blob" model proposed by Reitz was used,

which was equivalent to the diameter of the nozzle. The beginning of breakup was determined using the breakup length. The KH breakup of the liquid occurred within the breakup length; that is, the primary breakup occurred, and the breakup length was obtained by experiment. If the distance of a droplet from the nozzle was greater than the breakup length, the KH-RT hybrid model would be used to calculate the breakup of the droplet. Firstly, the RT model was used to determine whether the droplet broke. When the characteristic time of the droplet was larger than the breakup time scale of the RT model, RT breakup occurred. If the RT model did not cause the droplet to break, the KH model would be used to determine the droplet breaking.

In the KH model, fragmentation was only allowed when the droplet Weber number was greater than the critical Weber number. The radius of a droplet that breaks to produce a new droplet is:

$$r' = B_0 \Lambda_{KH}. \tag{7}$$

B_0 is the empirical constant, taken as 0.61. Λ_{KH} is the fastest growing KH wave, and Ω_{KH} is the maximum growth rate of a surface wave:

$$\Omega_{KH}\left(\frac{\rho_d r^3}{\sigma}\right)^{0.5} = \frac{\left(0.34 + 0.38 We_g^{1.5}\right)}{(1+Oh)\left(1+1.4T^{0.6}\right)}, \tag{8}$$

$$\frac{\Lambda_{KH}}{r} = 9.02\frac{\left(1+0.45Oh^{0.5}\right)\left(1+0.4T^{0.7}\right)}{\left(1+0.87We_g^{1.67}\right)^{0.6}}, \tag{9}$$

where r is the radius of a droplet, $Oh = We_d^{0.5}/Re_d$ is the Ohnesorge number of the liquid, $We_d = \rho_d r v^2/\sigma$ is the Weber number of the liquid, $We_g = \rho_g r v^2/\sigma$ is the Weber number of the gas, $Re_d = rv/\upsilon_d$ is the Reynolds number of the liquid, and $T = Oh \times We_g$.

During the liquid jet breakup, the diameter of the parent drop decreases due to mass loss. The rate of change in the radius of the parent drop is:

$$\frac{dr}{dt} = -\frac{(r-r')}{\tau_b}. \tag{10}$$

The breaking time τ_b is defined as:

$$\tau_b = \frac{3.726 B_1 r}{\Lambda_{KH}\Omega_{KH}}. \tag{11}$$

B_1 is the breakup time constant, which is between 1.732 and 40, and is taken as 15 in this paper.

The RT model was used to predict the growth of unstable waves on the droplet surface until the droplet broke up. The wavelengths of the fastest growing waves in the RT model are:

$$\Lambda_{RT} = \frac{2\pi C_{RT}}{K_{RT}}. \tag{12}$$

C_{RT} is an adjustable parameter related to the nozzle and is 0.1 in this paper. K_{RT} is the corresponding wave number:

$$K_{RT} = \sqrt{\frac{-g_d(\rho_d - \rho_g)}{3\sigma}}, \tag{13}$$

where g_d is the acceleration in the direction of the droplet trajectory.

When the wavelength is smaller than the droplet diameter, the RT wave grows on the droplet surface. The breakup time scale is calculated by predicting the frequency at which the droplet surface wave will grow most rapidly:

$$\tau_{RT} = \frac{C_\tau}{\Omega_{RT}}, \tag{14}$$

$$\Omega_{RT} = \sqrt{\frac{2}{3\sqrt{3\sigma}} \frac{\left[-g_d\left(\rho_d - \rho_g\right)\right]^{3/2}}{\rho_d + \rho_g}}, \tag{15}$$

where C_τ is an empirical constant, taken as 1.0.

The droplet breaks when the RT wave growth time is longer than the breaking time. The radius of the new droplet is:

$$r = 0.5\Lambda_{RT}. \tag{16}$$

3 Calculation model

Using the above atomization model, an experiment performed at Jiangsu University [51] was numerically simulated. The researchers used high-resolution laser shadowing to capture the flow field, and then used threshold segmentation to extract the atomization area of the jet. The penetration depth of spray refers to the vertical distance from the top boundary of the atomization area to the lower wall surface. Image software is used to obtain the penetration depth of the jet. The calculation area is 80 mm long and the cross-sectional area is 30 mm × 30 mm. A supersonic crossflow enters from the left side of the model. The distance of the injection position from the inlet is 15 mm. The Mach number is 2. The total pressure and temperature of the inlet flow are 0.8 MPa and 300 K, respectively. The diameter of the injected nozzle is 0.5 mm. The temperature of kerosene is 300 K. The angle between the jet and the inlet flow is 90°, and the droplet distribution is R-R. The calculation model is shown in Fig. 1. The calculation grid adopts a structured grid, and the mesh is refined near the nozzle and the wall surface. Six grids are evenly distributed at the nozzle. The mesh size of the first layer of the wall surface is 0.001 mm, ensuring that $y^+ \leqslant 1$. This paper studies the influence of liquid/gas momentum flux ratio and nozzle diameter on liquid jet atomization in a supersonic transverse flow. The calculation conditions and working conditions are shown in Table 1. Variable q

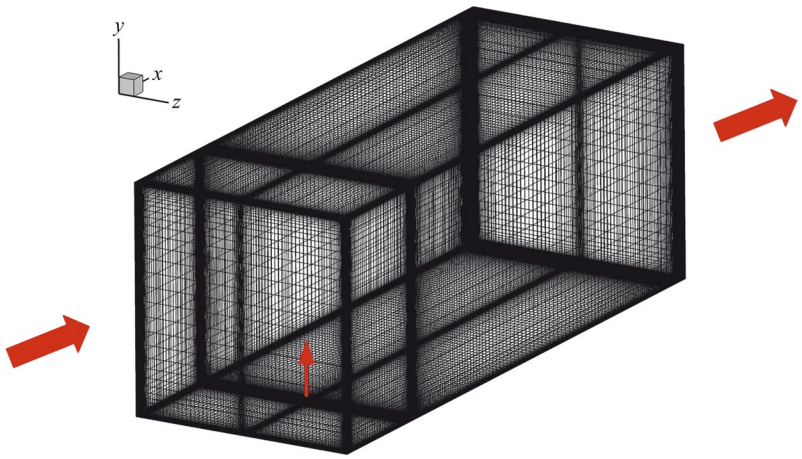

Fig. 1 Geometric model

Table 1 Computation condition

	Ma	P_t/MPa	T_t/K	*D*/mm	V_{inj}/(m/s)	*q*
Case 1	2	0.8	300	0.5	48	3.3
Case 2	2	0.8	300	0.5	59	4.8
Case 3	2	0.8	300	0.5	76	8
Case 4	2	0.8	300	0.3	48	3.3
Case 5	2	0.8	300	0.7	48	3.3

is the liquid-gas momentum flux ratio, which is defined as the ratio of the dynamic pressure of the fuel jet to the crossflow pressure. Its expression is given by Eq. (17).

$$q = \frac{\rho_d v_d^2}{\rho_g v_g^2}. \tag{17}$$

4 Results and discussion

4.1 Grid independence verification

In the numerical simulation, the precision of the grid has a significant influence on the accuracy of the calculation results. In this paper, the RANS method was used to simulate the transverse jet of kerosene in a supersonic airflow. The size and number of the mesh have a great influence on the calculation accuracy. To find a grid configuration that reduces the computational cost while maximizing the accuracy of the calculation, grid independence has been studied. 6 grids were uniformly distributed at the nozzle and kept unchanged. The settings of grid points in each direction and the total number of grids are shown in Table 2. A fixed time step of 1e-7s was chosen.

Figure 2a shows the jet penetration depth obtained from simulation results and from experimental results for different mesh sizes when the liquid/gas momentum flux ratio is 4.8 and the nozzle diameter is 0.5 mm. The numerical calculation defines the penetration

Table 2 Grid settings

	x	*y*	*z*	Grid numbers
Coarse grid	226	51	126	1,406,250
Medium Grid	286	71	146	2,892,750
Fine grid	302	91	166	4,469,850

depth of the jet as the maximum value of the *y*-coordinate after removing the outermost discrete droplets from the cross-section. When the grid quantity is 1.4 million, the error between the numerical results and the experimental results is large. The simulation results obtained using the 2.8 million grids and 4.4 million grids are in good agreement with the experimental results. In order to ensure the accuracy of the calculation results and save on computing resources, the model with 2.8 million grids was selected for the numerical simulation.

4.2 Atomization characteristic analysis

The numerical simulation results were compared with the experimental results to ensure the accuracy of the numerical simulation, as shown in Fig. 2b. Figure 2b shows the penetration depth of kerosene that issues from a nozzle with a diameter of 0.5 mm and a liquid/gas momentum flux ratio of 4.8. The solid line in red is the experimental value and the blue line is the simulation value. The jet penetration depth numerically simulated using the model in this paper is in good agreement with experiment. But in the area where the jet bends, our model overestimates the penetration depth of the jet. The reason for the large error at $x = 10 - 20$ mm is that on the one hand, the model itself simplifies the physical process, and on the other hand, the selection of model parameters is due to the uncertainty of the empirical parameters obtained under certain experimental conditions. Due to resolution reasons, the particles with smaller diameters on the outermost layer of the liquid mist may not be captured, which may cause the experimental penetration depth to be lower than the actual penetration depth. Overall, the numerical simulation of the liquid jet atomization process in the supersonic crossflow is reliable;

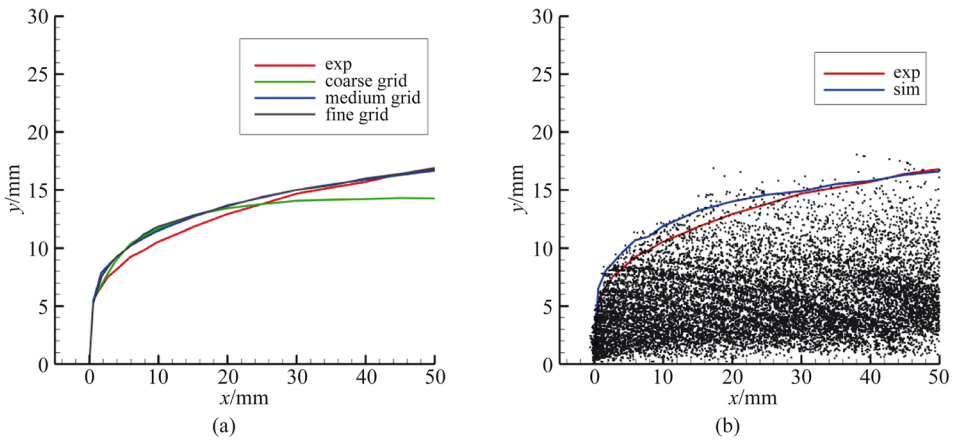

Fig. 2 Grid independence test and model validation

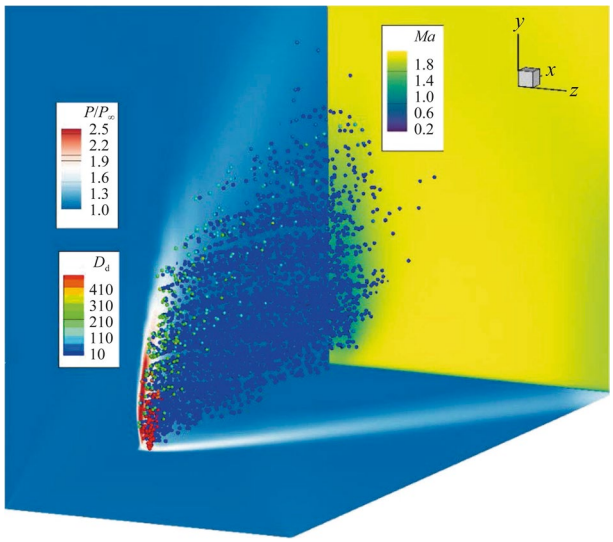

Fig. 3 3D flow field diagram of the jet

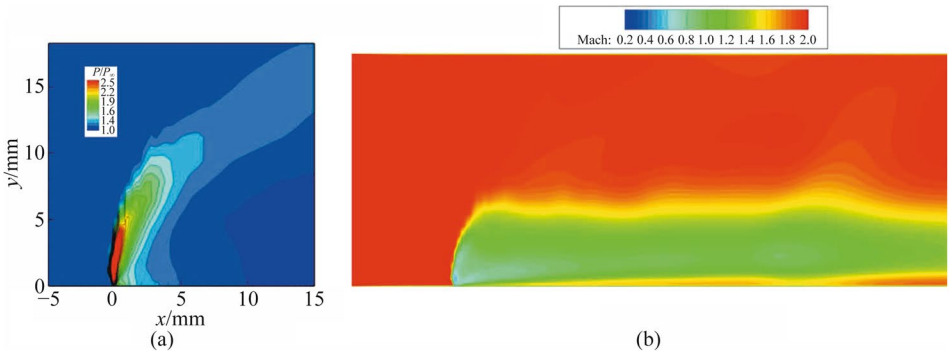

Fig. 4 The iso-contours of pressure and Mach number

it captures the trajectory of the liquid droplets more accurately by considering the KH breakup within the breakup length [12, 22, 47].

Figure 3 is a three-dimensional flow field diagram of the jet, showing the droplet distribution near the jet nozzle, the instantaneous pressure in the center plane and the wall-parallel plane, and the Mach number on the cross-section. The color of the particles represents the diameter of the droplet. As shown in Fig. 4, after large kerosene droplets enter the transverse airflow, the Mach number of the airflow in the center of the jet flow is low due to obstruction of the jet flow, and a bow shock wave is formed in front of the jet. And a high-pressure zone is formed in front of the jet, and there is a low-pressure zone inside the liquid mist zone. The size of a kerosene drop near the nozzle is equal to the diameter of the nozzle. When the jet moves upward, it is gradually deflected toward the direction of airflow under the action of the cross-flow. At some distance from the nozzle, within the breakup length, large droplets undergo KH unstable breakup, and small droplets continuously peel off on the surface of the droplets. These small droplets are then broken down into smaller droplets in the flow field. The competition between the KH unstable breakup and the RT

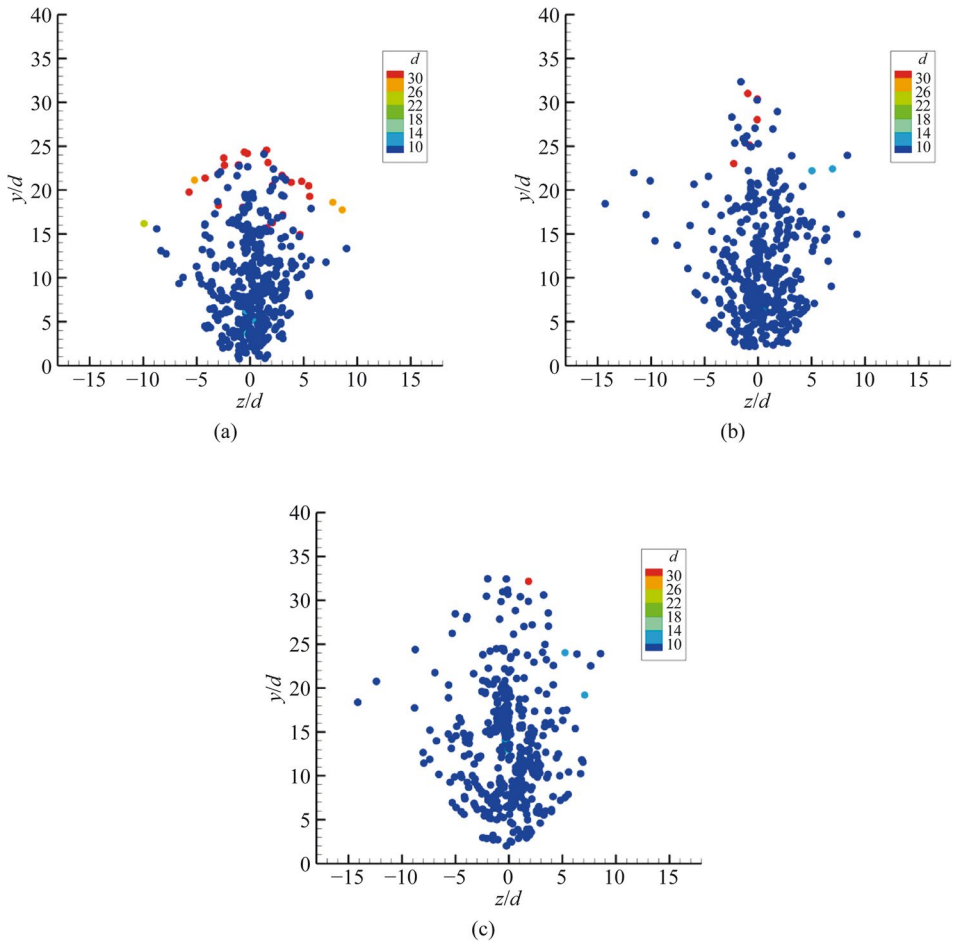

Fig. 5 Droplet distribution on different cross-sections. **a** $x/d = 20$, **b** $x/d = 60$, **c** $x/d = 120$

unstable breakup outside the breakup length promotes the continuous fragmentation of droplets.

Figure 5 shows the droplet distribution for different cross-sections in the flow field, where the droplet size is represented by color. The distribution of droplets on different cross-sections can be normalized by the diameter of the nozzle. Red represents larger droplets and blue represents smaller droplets. Comparing the droplet distributions on the $x/d = 120$ and $x/d = 20$ sections shows that, with the development of the kerosene jet, the droplet distribution increases in both penetration depth and spread direction. Moreover, the droplet distribution gradually disperses. In combination with Fig. 3, droplets with a larger diameter are distributed nearer to the jet nozzle and the upper surface of the jet. Since larger droplets have greater momentum and are less affected by the transverse airflow than smaller droplets, more of them penetrate the transverse airflow. Smaller droplets are more numerous and are distributed in the lower part of the jet. There are two ways to produce small droplets: one is the breakup of large droplets, and the other is the breakup of the liquid column due to shear on both sides [10, 46]. Therefore, a large number of small droplets are generated near the jet exit due to shear forces. With the development of the jet, and under the continuous interaction between the airflow and the droplets, large droplets are further broken into small droplets. The droplet

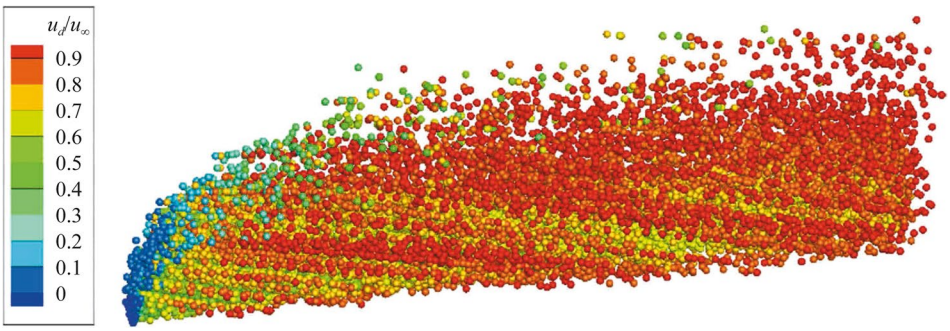

Fig. 6 Overall velocity distribution of the spray field

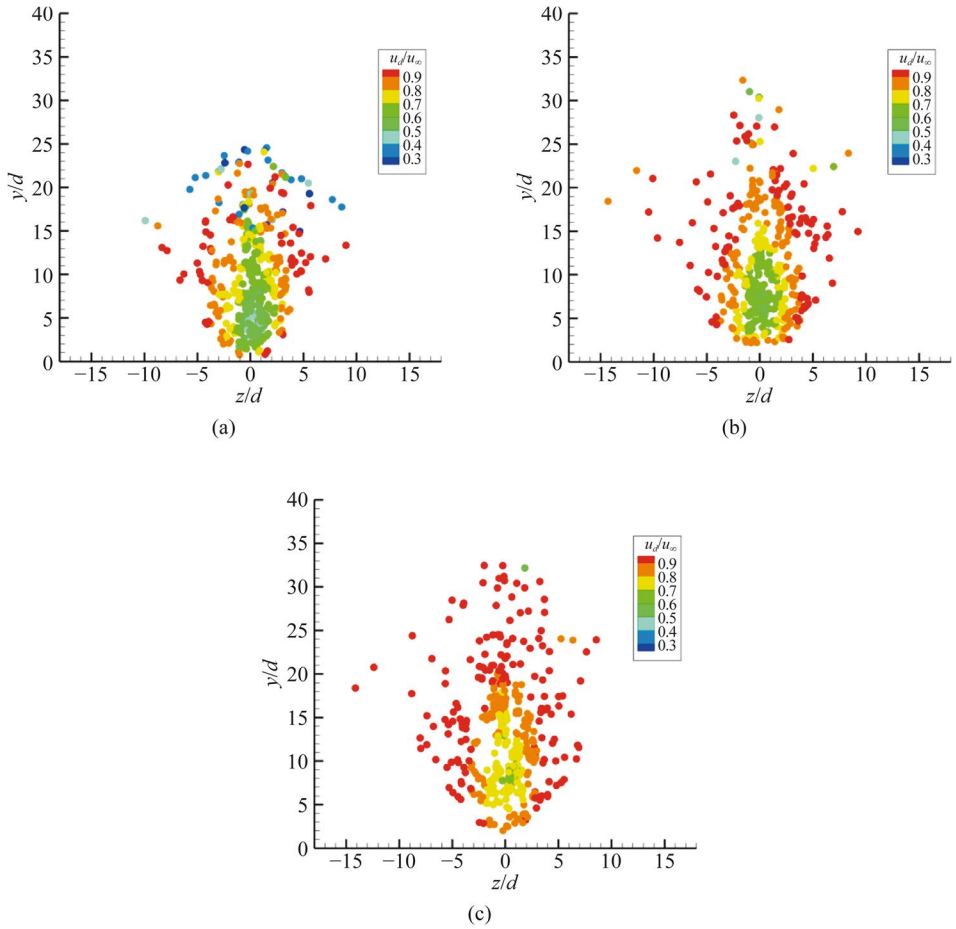

Fig. 7 Droplet velocity distribution on different cross-sections. **a** $x/d=20$, **b** $x/d=60$, **c** $x/d=120$

distribution on the $x/d=120$ cross-section shows that the droplet diameter distribution in the exit area is relatively uniform.

Figure 6 shows the overall droplet distribution (droplets are colored by flow velocity). Figure 7 shows the droplet velocity distribution on different cross-sections. After kerosene droplets of equal diameter are injected into the supersonic transverse flow field from the nozzle, they are broken down into smaller droplets under the action of the

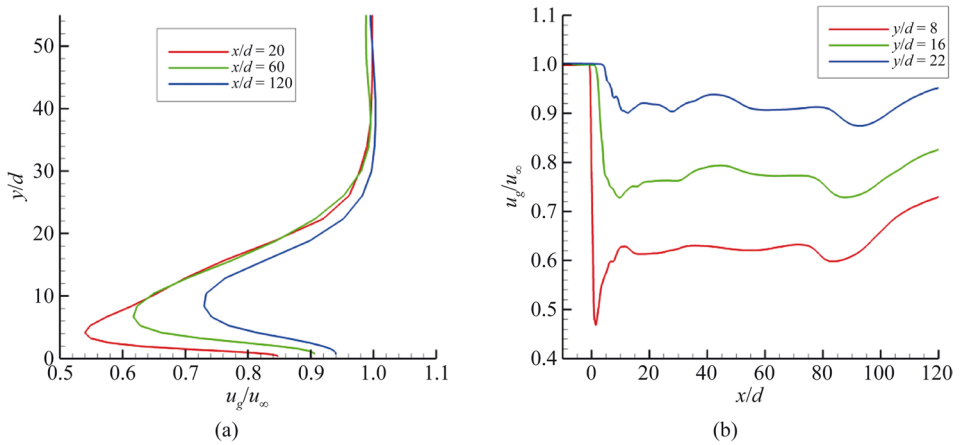

Fig. 8 Gas velocity distribution at different positions

high-speed airflow; these smaller droplets are then rapidly accelerated. Figures 6 and 7 show that the droplet velocity is lower on the upper surface and in the core region of the jet and larger on the periphery of the jet. This may be because the droplets around the jet are relatively sparse, making it easier for them to interact with the surrounding airflow and break, resulting in a smaller droplet size. Small droplets have small inertia and are easily accelerated by the airflow, resulting in higher droplet velocities under aerodynamic forces. The droplets at the center of the jet are relatively dense and have a strong blocking effect on the incoming flow. The velocity of the airflow at the center of the mist is lower than that at the periphery of the jet, as shown in Fig. 8. Therefore, the velocity of the droplets at the core of the jet is relatively low. With the development of the jet and the diffusion of the droplet, the interaction between the droplet and the air at the center of the jet is enhanced, meaning that the droplet speed gradually increases.

Figure 8a shows the gas velocity distribution along the flow direction on the central section. The velocity at different positions is dimensionless based on the velocity of the incoming flow. In the jet area, due to the obstruction of the jet in the jet area, the gas phase velocity significantly decreases and there is a minimum velocity. The number of particles in the near wall area is relatively small, so the velocity of the airflow around the jet column quickly recovers, resulting in a higher airflow velocity in the near wall area. With the development of the jet flow, the lifting effect of the airflow on the jet is enhanced. The gas phase velocity at $x/d = 120$ is larger than that at $x/d = 60$, and the position of the minimum airflow velocity gradually increases. In the core of the jet, which is slightly away from the wall, the number of particles in the jet is relatively dense, and the obstruction effect on the airflow gradually increases, resulting in the lowest gas velocity. Along the development of the jet column, the gas velocity gradually tends to the inlet velocity due to the breakup and dispersion of droplets. At $x/d = 120$ downstream of the jet, due to the atomization of the droplets and the acceleration effect of the airflow on the droplets, the minimum of the gas velocity increases, that is, the air velocity increases, corresponding to the increase in droplet velocity in Fig. 7. Figure 8b shows the gas velocity distribution at different penetration depths on the central section. Due to the obstruction effect of the jet on the airflow, a bow shock wave is formed in front of the

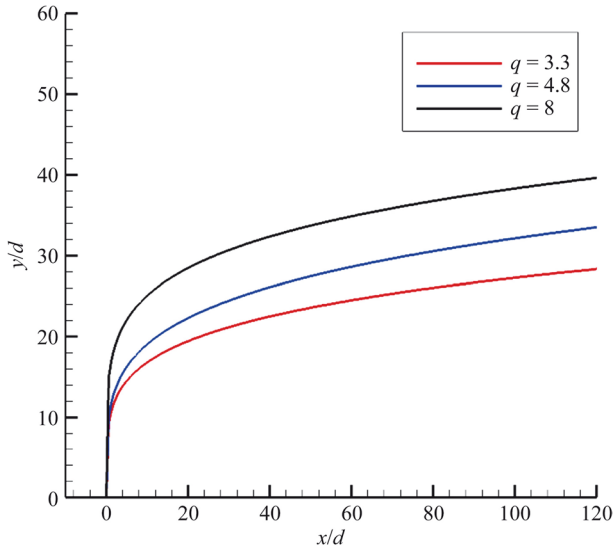

Fig. 9 The effect of liquid-gas momentum flux ratio on liquid penetration

jet flow. After passing through the bow shock wave, the speed of the airflow decreases rapidly, especially near the wall at $y/d = 8$. With the development of the jet, the jet speed gradually increases under the action of the airflow, and the airflow speed also increases. The airflow velocity in the exit area is close to the incoming velocity. As the penetration depth y increases, the intensity of the bow shock decreases, and the airflow velocity gradually recovers. This explains the higher the velocity of a droplet, the nearer it is to the jet periphery.

4.3 Influence of liquid/gas momentum flux ratio on kerosene jet atomization characteristics

The penetration depth of a kerosene jet is a key parameter in the characterization of the mixing characteristics of fuel and air in transverse airflows. The momentum flux ratio is the parameter most widely used to describe the atomization characteristics of fuel jets in transverse airflows. It is also the main control parameter of jet penetration depth [9, 52]. In order to achieve a better atomization effect, the jet velocity is usually increased by increasing the liquid/air momentum flux ratio q while the inflow conditions remain unchanged, in order to increase the penetration depth of the jet. The influence of q on atomization is analyzed below.

Figure 9 shows the penetration depth of the kerosene jet for different liquid/gas momentum flux ratios q when the nozzle diameter is 0.5 mm. The penetration depth of the kerosene jet for $q = 8$ is the largest, and that for $q = 3$ is the smallest. For a given set of incoming flow conditions, the larger the momentum flux ratio, the larger the initial velocity of the liquid column; the jet reaches a greater distance in the same time, and the penetration depth increases accordingly. Therefore, as q increases, the penetration depth of the jet increases.

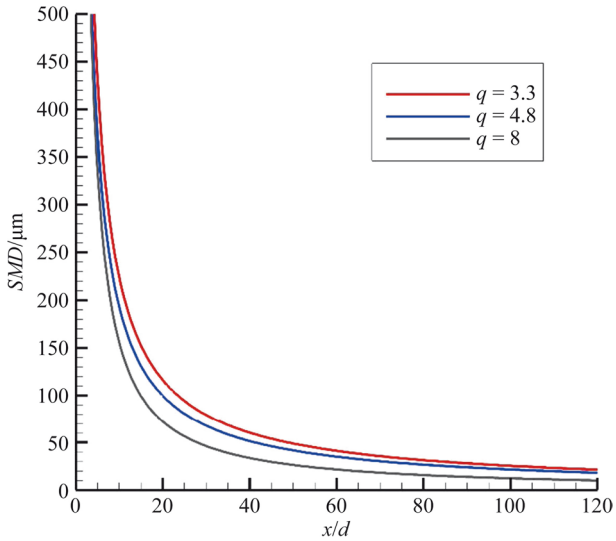

Fig. 10 The effect of liquid-gas momentum flux ratio on SMD distribution

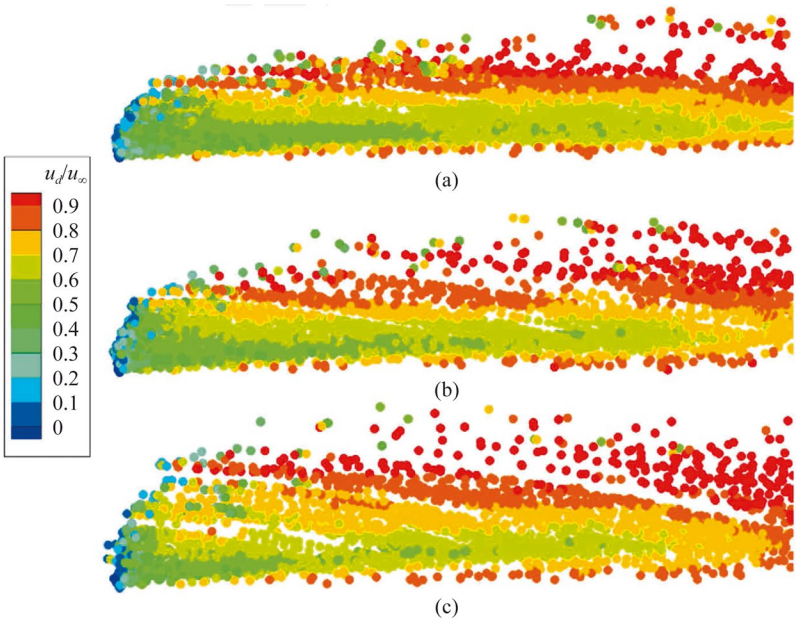

Fig. 11 The effect of liquid-gas momentum flux ratio on particle velocity distribution. **a** $q=3.3$, **b** $q=4.8$, **c** $q=8$

Figure 10 shows the SMD distribution of a jet along the flow direction. Figure 11 shows the central plane velocity distribution of the kerosene jet for different momentum flux ratios. Figure 10 shows that the droplet SMD near the nozzle is large for the three momentum flux ratios, and that the particles are quickly broken down due to aerodynamic forces after it is ejected from the nozzle. The droplet size suddenly decreases. With the development of the jet, the change in droplet size

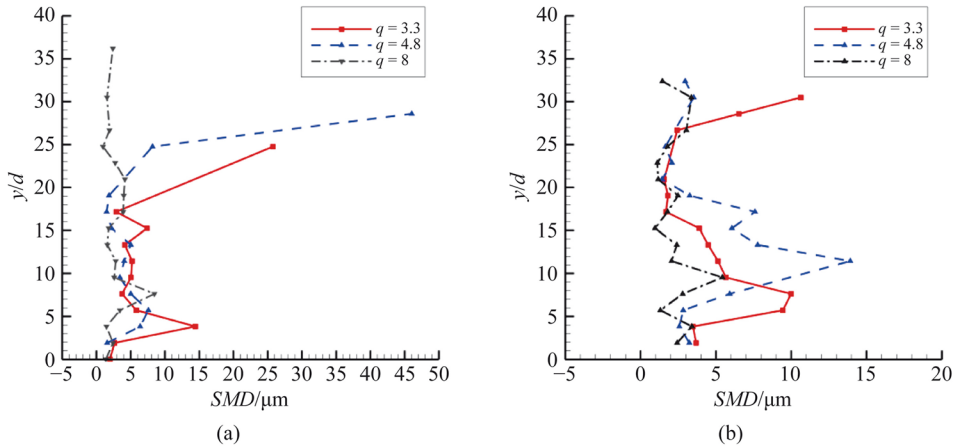

Fig. 12 SMD distribution on different cross-sections. **a** $x/d=60$, **b** $x/d=120$

slows down and eventually becomes stable. Jet atomization in the high-speed airflow essentially ends within a short distance, and droplet fragmentation is mainly affected by aerodynamic forces. At the same x, the SMD of $q=8$ is smaller than the SMD of $q=3.3$. This is because, as the liquid/gas momentum flux ratio increases, the initial momentum of the jet increases, and the jet reaches farther within the same time. In the same region, the number of kerosene droplets at the center of the jet with a high momentum flux ratio is less than that of a jet with a low momentum flux ratio, as shown in Fig. 11. Droplets are more likely to interact with the incoming flow and break into smaller droplets. Figure 11 shows that the momentum flux ratio has little influence on the velocity distribution of droplets. The droplet velocity at the near wall, peripheral, and far field of the jet is higher under the three momentum flux ratios. In the central plane velocity distribution, the low-velocity region of $q=8$ is shorter than that of $q=3.3$, and the particle distribution is sparser. Therefore, the droplet SMD for the kerosene jet with a momentum flux ratio of 8 is smaller.

Figure 12 shows the particle size distribution of different liquid/gas momentum flux ratios at different cross-sections on the central plane. Changes in the SMD in the direction of the jet are roughly S-shaped for different values of q. Approaching the wall, the SMD decreases because of shear forces and the trailing phenomenon of the liquid jet. During trailing, because of the pressure gradient caused by the bow shock wave formed by the transverse airflow in front of the jet column, small liquid droplets formed during catastrophic breakup of the liquid jet are brought close to the wall. Due to the shear action of the airflow, a large number of small droplets are produced by stripping on both sides of the liquid column. Small droplets have small momentum, good airflow following, and do not change direction easily, meaning that they are found near the wall. The medium y value corresponding to a large SMD may correspond to the bottom location where the droplet is more dense. Here, the droplets are large because the interaction between them and the airflow is weak. With the development of the jet, the SMD decreases with increasing y due to the continuous, strong, shear effect of the airflow. At $x/d=60$, jet atomization is basically complete. Except for a small number of droplets with a large diameter on the upper surface of the jet, the SMD of the jet is about 10 μm. With changes in q and x cross-sections, the SMD changes relatively little, which is due to the

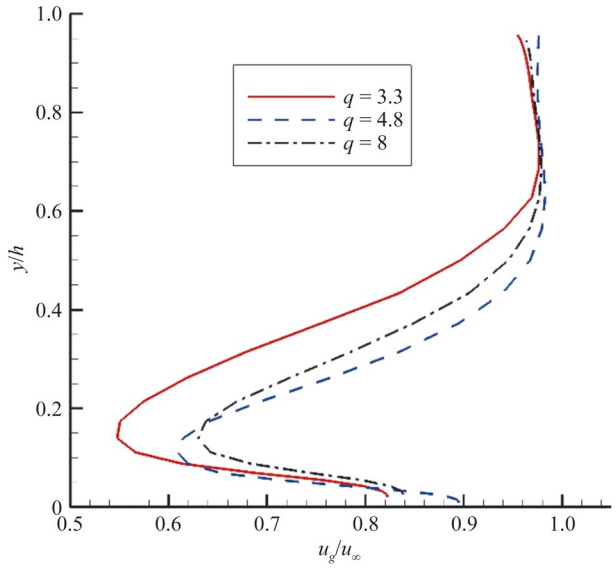

Fig. 13 The effect of liquid-gas momentum ratio on gas velocity distribution

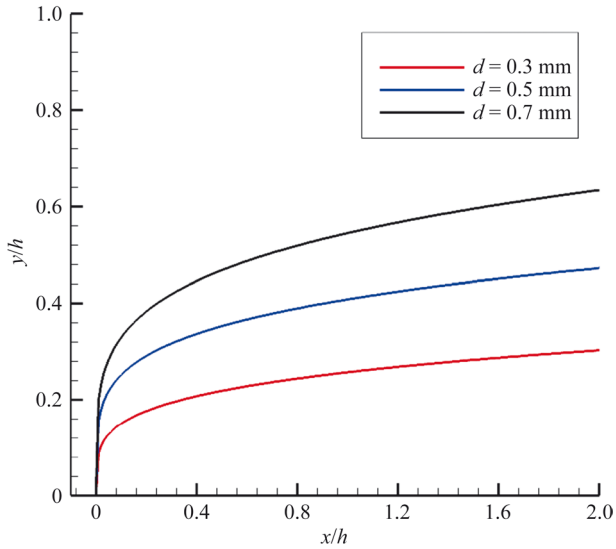

Fig. 14 The effect of nozzle diameter on liquid penetration

dominance of the aerodynamic force of the transverse flow during atomization. Figure 13 shows the gas velocity distribution for different liquid/gas momentum flux ratios at the central cross-section $x/d=60$. The gas phase velocity distribution has an inverse S-shape. The results show that the minimum value of the gas velocity gradually increases with increasing liquid/gas momentum flux ratio. This is consistent with the previous proposal that the jet center with a high momentum flux ratio is sparse and the gas velocity is higher.

4.4 Influence of nozzle diameter on kerosene jet atomization characteristics

Nozzle diameter is also a factor affecting atomization. Figure 14 shows the penetration depth for a given liquid/gas momentum flux ratio $q=3.3$, and

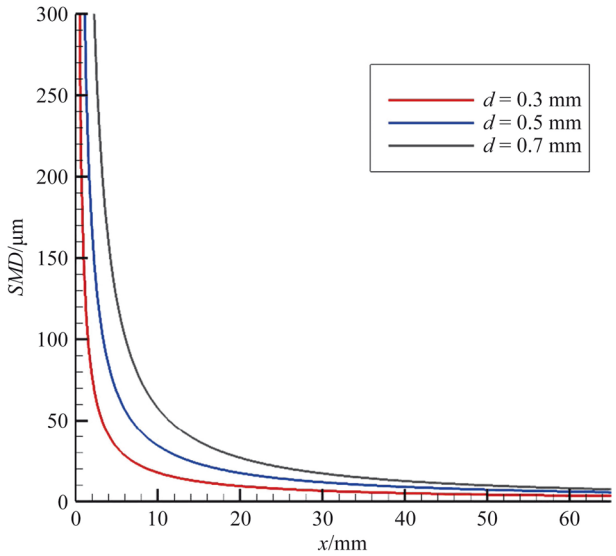

Fig. 15 The effect of nozzle diameter on SMD distribution

different nozzle diameters. The penetration trajectory is normalized by the height of the model entrance. The results indicate that the penetration depth increases with increasing nozzle diameter. For a given set of incoming flow conditions, a constant liquid/gas momentum flux ratio means that the initial velocity of the kerosene jet is constant. The kerosene jet with a larger nozzle diameter has a higher Reynolds number, mass flow rate, and momentum, resulting in a stronger penetration ability. It takes longer for the transverse airflow to change the direction of the jet for a larger mass flow than for a smaller mass flow. Therefore, a kerosene jet with a larger nozzle diameter penetrates more deeply.

Figure 15 shows the SMD distribution along the flow line for different nozzle diameters. For a given value of x, the smaller the diameter of the jet hole, the smaller the SMD of the jet. The smaller the size of the droplet ejected from the nozzle, the smaller the Weber number of the droplet. Under the action of aerodynamic forces from the incoming airflow, small particles break more easily than large particles. The atomization is more uniform. Figure 16 shows the distribution of droplet velocity under different nozzle diameters on the central plane. The velocity of the jet center plane with a nozzle diameter of 0.7 mm is lower than that of the jet center plane with a nozzle diameter of 0.3 mm, and the droplet distribution is more discrete. This is because the larger the jet hole diameter, the larger the droplet inertia, and the farther the jet reaches the position within the same time. Breaking into small droplets of the same size, a jet with a larger nozzle diameter requires longer time and a longer distance. Therefore, the distribution of droplets on the central plane of the jet with a larger nozzle diameter is more dispersed, and the low-velocity zone of the liquid core is longer.

Figure 17 shows the particle size distribution of different hole diameters at different sections on the jet center plane. For a given liquid/gas momentum flux ratio, the SMD of different nozzle diameters is S-shaped. Droplets with a smaller nozzle diameter have a lower penetration depth, a smaller size range, and more uniform

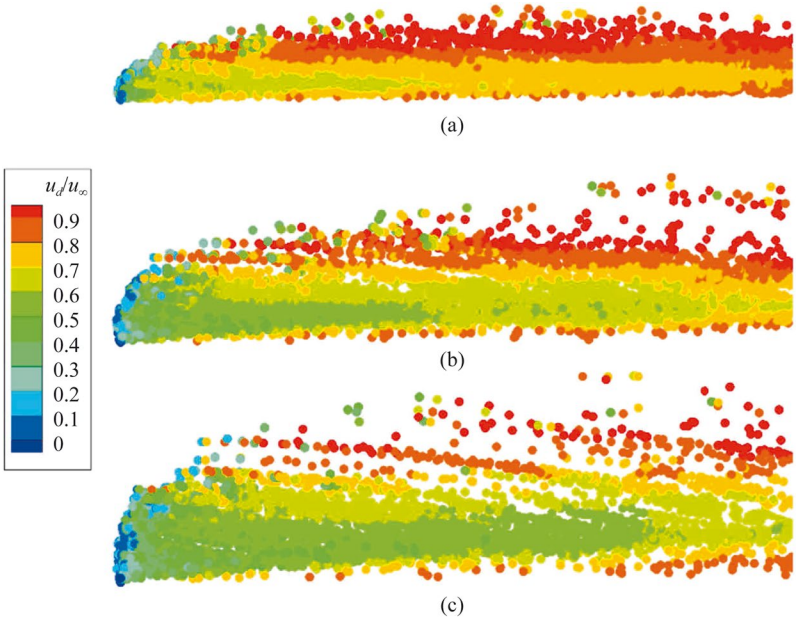

Fig. 16 The effect of nozzle diameter on particle velocity distribution. **a** $d = 0.3$ mm, **b** $d = 0.5$ mm, **c** $d = 0.7$ mm

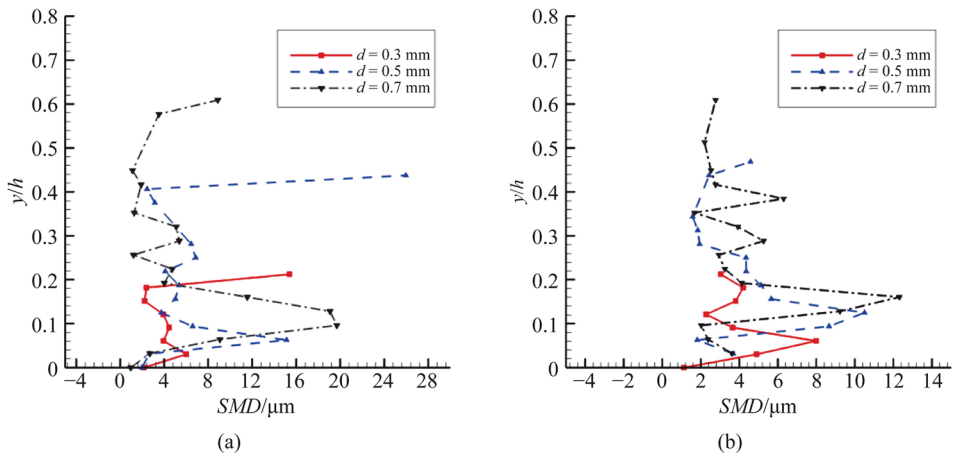

Fig. 17 SMD distribution on different cross-sections. **a** $x = 30$ mm, **b** $x = 60$ mm

distribution. Because the droplets in the core region of the jet are relatively dense and surrounded by surrounding droplets, and the interaction with the airflow is weak, the SMD in the core region of the jet near the wall is large. With increasing nozzle diameter, the SMD near the wall increases. The position of the larger SMD is elevated with increasing nozzle diameter. At $x = 30$ mm, the jet SMD for different hole diameters is all below 30 μm. The SMD of jets with $x = 60$ mm is below 10 μm. Figure 18 shows the gas velocity distribution of the $x = 30$ mm section on the central plane under different nozzle diameters. For a given value of y, the airflow with a nozzle diameter of 0.7 mm has the lowest velocity. As the diameter of the nozzle decreases, the droplet is more easily accelerated by the airflow, and the minimum

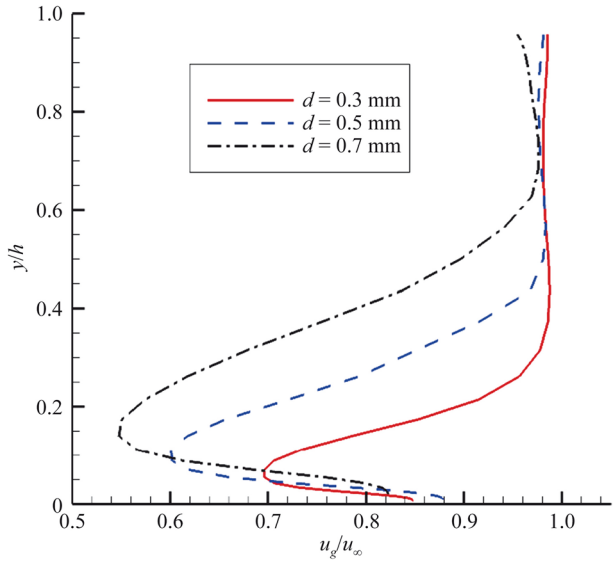

Fig. 18 The effect of nozzle diameter on gas velocity distribution

gas velocity increases gradually. The mass flow rate of a kerosene jet with a small diameter is less, the blocking effect of the jet on the airflow is weakened, and the penetration depth of the jet is therefore reduced. The height of the minimum point of the gas velocity gradually decreases.

5 Conclusion

In this paper, the atomization of a kerosene jet in a supersonic airflow was numerically simulated using the Euler-Lagrange method. The Reitz wave model was used to simulate the surface fragmentation of the jet, and the improved KH-RT hybrid model was used to simulate the secondary breakup of a droplet. The numerical simulation of the spray structure of a kerosene jet considering the surface breakup process within the breakup length was in good agreement with the experimental results. After the jet was injected into the supersonic crossflow, the droplet broke and was quickly deflected by aerodynamic forces. Near the jet nozzle, the size of the droplet was equal to the nozzle, and the droplet velocity along the flow direction was low. Therefore, the droplet size formed by the primary breakup was large, and the droplet distribution was relatively dense. With the development of the jet flow, large droplets broke into small droplets under the action of the crossflow. The droplet distribution gradually dispersed, and the droplet size gradually decreased, becoming uniform.

Analyzing the influence of the liquid/gas momentum flux ratio on the atomization characteristics of the jet showed that the penetration depth of the jet increased with increasing momentum flux ratio. The interaction between the airflow and the droplet was stronger at higher momentum flux ratios. This was because the droplet density of the jet with a high momentum flux ratio is lower than that of the droplet with a low momentum flux ratio, making it easier for the airflow and droplets to interact with each other. Therefore, the droplets broke up quickly, the SMD of droplets in the flow field was small, and the droplet velocity in the flow field was large. At $x/d = 60$, all jets were basically atomized, and the SMD of the jet was around 10 μm.

For a given liquid/gas momentum flux ratio, the penetration depth and the SMD increased with the nozzle diameter. The SMD of three different nozzle diameters at $x = 30$ mm was below 30 μm, and the SMD of the jet at $x = 60$ mm was below 10 μm. Compared with the liquid/gas momentum flux ratio, the increase in nozzle diameter contributed more significantly to the penetration depth. Therefore, for a given set of incoming flow conditions, increasing the liquid/gas momentum flux ratio and decreasing the diameter of the jet hole were conducive to jet breakup and atomization.

Acknowledgements
The authors would like to thank Dr. Shunhua Yang for his assistance in the paper writing process.

Authors' contributions
Jialing Le: Conceptualization and Methodology; Ye Tian: Review and Editing; Yi Zhang: Simulation. All authors read and approved the final manuscript.

Funding
This project was supported by the Youth Independent Innovation Science Foundation of the Aerospace Technology Institute of China Aerodynamics Research and Development Center (Grant No. QNJJ23031).

Availability of data and materials
The data that support the findings of this study are available from the corresponding author upon reasonable request.

Declarations

Competing interests
The authors declare that there are no conflicts of interest regarding the publication of this paper.

Received: 6 September 2023 Accepted: 8 November 2023
Published online: 18 February 2024

References

1. Huang W, Tan J, Liu J et al (2015) Mixing augmentation induced by the interaction between the oblique shock wave and a sonic hydrogen jet in supersonic flows. Acta Astronaut 117:142–152
2. Urzay J (2018) Supersonic combustion in air-breathing propulsion systems for hypersonic flight. Annu Rev Fluid Mech 50:593–627
3. Park JH, Yoon Y, Hwang SS (2002) Improved TAB model for prediction of spray droplet deformation and breakup. Atom Sprays 12:387–401
4. Bhatia B, Johny T, De A (2023) Understanding the liquid jet break-up in various regimes at elevated pressure using a compressible VOF-LPT coupled framework. Int J Multiph Flow 159:104303
5. Kush EA Jr, Schetz JA (1973) Liquid jet injection into a supersonic flow. AIAA J 11:1223–1224
6. Ren Z, Wang B, Xiang G et al (2019) Supersonic spray combustion subject to scramjets: progress and challenges. Prog Aerosp Sci 105:40–59
7. Wu PK, Kirkendall KA, Fuller RP et al (1998) Spray structures of liquid jets atomized in subsonic crossflows. J Propul Power 14:173–182
8. Kush EA Jr, Schetz JA (1972) Liquid jet injection into a supersonic flow. In: 8th joint propulsion specialist conference, New Orleans, 29 November-1 December 1972
9. Wei X, Li L, Zhao Z et al (2020) The droplet size and penetration height of a kerosene jet in a crossflow. Atom Sprays 30:495–515
10. Wu L, Wang Z, Li Q et al (2015) Investigations on the droplet distributions in the atomization of kerosene jets in supersonic crossflows. Appl Phys Lett 107:104103
11. Kolpin MA, Horn KP, Reichenbach RE (1968) Study of penetration of a liquid injectant into a supersonic flow. AIAA J 6:853–858
12. Reitz RD, Diwakar R (1987) Structure of high-pressure fuel sprays. SAE Tech Paper 870598
13. O'Rourke PJ, Amsden AA (1987) The TAB method for numerical calculation of spray droplet breakup. SAE Tech Paper 872089
14. Reitz RD (1988) Modeling atomization processes in high-pressure vaporizing spray. Atom Sprays 3:309–337
15. Patterson MA, Reitz RD (1998) Modeling the effects of fuel spray characteristics on diesel engine combustion and emission. SAE Tech Paper 980131
16. Wang J, Liu C, Wu Y (2010) Numerical simulation of spray atomization in supersonic flows. Mod Phys Lett B 24:1299–1302
17. Saeedipour M, Pirker S, Bozorgi S et al (2016) An Eulerian–Lagrangian hybrid model for the coarse-grid simulation of turbulent liquid jet breakup. Int J Multiph Flow 82:17–26
18. Saeedipour M, Schneiderbauer S, Plohl G et al (2017) Multiscale simulations and experiments on water jet atomization. Int J Multiph Flow 95:71–83
19. Huang J, Zhao X, Jiang H (2021) Numerical simulation of the atomization of liquid transverse jet in supersonic airflow. Phys Fluids 33:052114

20. Liu L, Yang L, Fu Q (2020) Droplet size spatial distribution model of liquid jets injection into subsonic crossflow. Int J Aerosp Eng 2020:9317295
21. Fan X, Wang J, Zhao F et al (2018) Eulerian-Lagrangian method for liquid jet atomization in supersonic crossflow using statistical injection model. Adv Mech Eng 10:1–13
22. Reitz RD, Diwakar R (1987) Structure of high-pressure fuel sprays. SAE Trans 96:492–509
23. Lin KC, Kennedy PJ, Jackson TA (2004) Structures of water jets in a Mach 1.94 supersonic crossflow. In: 42nd AIAA aerospace sciences meeting and exhibit, Reno, 5-8 January 2004
24. Lin KC, Kennedy P, Jackson TA (2000) Spray penetration heights of angle-injected aerated-liquid jets in supersonic crossflows. In: 38th aerospace sciences meeting and exhibit, Reno, 10-13 January 2000
25. Im KS, Lin KC, Lai MC (2005) Spray atomization of liquid jet in supersonic cross flows. In: 43rd AIAA aerospace sciences meeting and exhibit, Reno, 10-13 January 2005
26. Beale JC, Reitz RD (1999) Modeling spray atomization with the Kelvin-Helmholtz/Rayleigh-Taylor hybrid model. Atom Sprays 9:623–650
27. Wang YQ, Xiao F, Lin S et al (2021) Numerical investigation of droplet properties of a liquid jet in supersonic crossflow. Int J Aerosp Eng 2021:8828015
28. Li P, Wang Z, Bai X et al (2019) Three-dimensional flow structures and droplet-gas mixing process of a liquid jet in supersonic crossflow. Aerosp Sci Technol 90:140–156
29. Li P, Wang H, Sun M et al (2021) Numerical study on the mixing and evaporation process of a liquid kerosene jet in a scramjet combustor. Aerosp Sci Technol 119:107095
30. Li P, Wang Z, Sun M et al (2017) Numerical simulation of the gas-liquid interaction of a liquid jet in supersonic crossflow. Acta Astronaut 134:333–344
31. Huang W, Yan L (2013) Progress in research on mixing techniques for transverse injection flow fields in supersonic crossflows. J Zhejiang Univ Sci A 14(8):554–564
32. Wei Huang (2018) Mixing enhancement strategies and their mechanisms in supersonic flows: a brief review. Acta Astronaut 145:492–500
33. Wei Huang (2016) Transverse jet in supersonic crossflows. Aerosp Sci Technol 50:183–195
34. Wei Huang (2019) Supersonic mixing in airbreathing propulsion systems for hypersonic flights. Prog Aerosp Sci 109:100545
35. Huang W, Du ZB, Yan L et al (2018) Flame propagation and stabilization in dual-mode scramjet combustors: a survey. Prog Aerosp Sci 101:13–30
36. Su YH, Yuan HF, Su YP (2020) Liquid-fuel injection into supersonic cross flow. Combust Sci Technol 192:1436–1447
37. Pan Y, Dai JF, Bao H (2014) Effect of scramjet combustor configuration on the distribution of transverse injection kerosene. J Mech Sci Technol 28:4997–5002
38. Yang H, Li F, Sun BG (2012) Trajectory analysis of fuel injection into supersonic cross flow based on schlieren method. Chin J Aeronaut 25:42–50
39. Mashayek A, Behzad M, Ashgriz N (2011) Multiple injector model for primary breakup of a liquid jet in crossflow. AIAA J 49:2407–2420
40. Mashayek A, Ashgriz N (2009) Model for deformation of drops and liquid jets in gaseous crossflows. AIAA J 47:303–313
41. Mashayek A, Jafari A, Ashgriz N (2008) Improved model for the penetration of liquid jets in subsonic crossflows. AIAA J 46:2674–2686
42. Yu S, Yin B, Bi Q et al (2021) The influence of elliptical and circular orifices on the transverse jet characteristics at supersonic crossflow. Acta Astronaut 185:124–131
43. Sathiyamoorthy K, Danish TH, Iyengar VS et al (2020) Penetration and combustion studies of Tandem liquid jets in supersonic crossflow. J Propul Power 36:920–930
44. Lin KC, Kennedy PJ, Jackson TA (2002) Penetration heights of liquid jets in high-speed crossflows. In: 40th AIAA aerospace sciences meeting & exhibit, Reno, 14-17 January 2002
45. Costa M, Melo MJ, Sousa JMM et al (2006) Spray characteristics of angled liquid injection into subsonic crossflows. AIAA J 44:646–653
46. Almeida H, Sousa JMM, Costa M (2014) Effect of the liquid injection angle on the atomization of liquid jets in subsonic crossflows. Atom Sprays 24:81–96
47. Yang S, Le J, Zhao H et al (2009) Three-dimensional massively parallel numerical simulation of kerosene-fueled scramjet. Chin J Comput Phys 26:534–540 (in Chinese)
48. Xing JW, Xiao BG (2012) Numerical simulation of H_2O vitiation effects on kerosene-fueled scramjet combustor performance. J Aerosp Power 27:2408–2413 (in Chinese)
49. Ou M, Yan L, Huang W et al (2018) Detailed parametric investigations on drag and heat flux reduction induced by a combinational spike and opposing jet concept in hypersonic flows. Int J Heat Mass Transfer 126:10–31
50. Kumaran K, Badu V (2009) Mixing and combustion characteristics of kerosene in a model supersonic combustor. J Propul Power 25:583–592
51. Yu S, Yin B, Deng W, et al (2018) Internal flow and spray characteristics for elliptical orifice with large aspect ratio under typical diesel engine operation conditions. Fuel 228:62–73
52. Broumand M, Birouk M (2016) Liquid jet in a subsonic gaseous crossflow: recent progress and remaining challenges. Prog Energy Combust Sci 57:1–29

Publisher's Note